EDGE ARTICLE

Photocurrent of BiVO₄ is limited by surface recombination, not surface catalysis†

Carolin Zachäus,‡[a] Fatwa F. Abdi,‡*[a] Laurence M. Peter[b] and Roel van de Krol*[a]

Bismuth vanadate is one of the most promising photoanode materials for photoelectrochemical water splitting. In order to achieve high photocurrents the surface of BiVO₄ always has to be modified with water oxidation catalysts, such as cobalt phosphate (CoPi), FeOOH, or NiFeO$_x$. While this has generally been attributed to the poor intrinsic catalytic activity of BiVO₄, detailed insight into the fate of the photogenerated charge carriers at the surface is still lacking. We used intensity modulated photocurrent spectroscopy (IMPS) to investigate the surface carrier dynamics of bare and CoPi-modified spray-deposited BiVO₄ films. Using a model developed by Peter *et al.*, it was possible to distinguish the reaction rate constants for surface recombination and charge transfer to the electrolyte. We found that modification with CoPi reduced the surface recombination of BiVO₄ with a factor of 10–20, without significantly influencing the charge transfer kinetics. Control experiments with RuO$_x$, one of the best known OER electrocatalysts, did not affect surface recombination and led to an actual decrease of the photocurrent. These results show that the main role of the CoPi is to passivate the surface of BiVO₄ and that, contrary to earlier assumptions, the photocurrent of BiVO₄ is limited by surface recombination instead of charge transfer. The importance of surface recombination is well recognized for conventional semiconductors in the field of photovoltaics; these findings show that it may also play a crucial role in oxide-based semiconductors for photoelectrochemical energy conversion.

Introduction

The potential application of metal oxides as semiconductor photoelectrodes for water splitting critically depends on the development of efficient, inexpensive water oxidation catalysts to enhance the surface reaction kinetics. For example, BiVO₄—currently the most promising metal oxide photoanode—suffered from having low hole transfer efficiency for a long time,[1,2] but this problem has been shown to be easily solved by modifying its surface with CoPi, RhO₂, FeOOH, NiFeO$_x$, or MnO$_x$ catalysts.[2–6] In the past few years, many more studies on modified semiconductor surfaces have been reported. A particularly versatile example is cobalt phosphate (CoPi), a water oxidation catalyst that was initially developed by Nocera and co-workers[7] and has been shown to greatly enhance the photocurrents of *e.g.*, Fe₂O₃,[8–11] WO₃,[12] BiVO₄,[5,13,14] and TaON.[15,16] Despite these successes, the true nature of the enhancement is unclear. In BiVO₄ it is usually assumed that the low charge injection

efficiency is related to the poor surface catalytic activity of the material, but this is not necessarily true. For example, a high density of surface recombination centers can also lead to a low charge injection efficiency. This raises some intriguing questions: (i) what really limits the charge injection efficiency in BiVO₄? (ii) How do the so-called co-catalysts solve the charge injection problem: is it a true catalytic effect or passivation of surface recombination centers? (iii) What is the mechanism behind the improvement in photocurrent?

A few years ago, Gamelin pointed out that there are two conflicting views on the mechanism of photocurrent enhancement in the same CoPi/hematite (α-Fe₂O₃) photoanode system.[8] Barroso *et al.* reported enhanced charge separation and carrier life time in the semiconductor by introducing CoPi,[9] which was attributed to increased band bending. In contrast, Klahr *et al.* found no indications for a change in band bending, and instead suggested that CoPi rapidly extracts photogenerated holes from hematite, thereby reducing the electron–hole recombination at the surface.[17] Boettcher and co-workers made a first general attempt to reconcile these observations by proposing the concept of an 'adaptive' junction.[18] They showed that redox-active ion-permeable electrocatalysts (*e.g.*, NiOOH and possibly CoPi) yield 'adaptive' semiconductor/electrocatalyst junctions where the effective Schottky barrier height changes dynamically with potential as a consequence of changes in the oxidation state of the electrocatalyst. Even before these studies,

[a]*Helmholtz-Zentrum Berlin für Materialien und Energie GmbH, Institute for Solar Fuels, Hahn-Meitner-Platz 1, 14109 Berlin, Germany. E-mail: fatwa.abdi@helmholtz-berlin.de; roel.vandekrol@helmholtz-berlin.de*

[b]*Department of Chemistry, University of Bath, Bath BA2, 7AY, UK*

‡ Equal contribution.

Zhong and Gamelin already suggested that CoPi reduces the surface recombination of BiVO$_4$.[5] However, their experiments could not distinguish whether the increase in photocurrent was indeed due to a decrease in surface recombination, or to enhanced oxygen evolution kinetics.

These considerations illustrate that further studies are needed to understand the role of CoPi—and co-catalysts in general—on a semiconductor photoanode for water oxidation. We consider three different roles for a co-catalyst. First, it can improve the water oxidation kinetics by reducing the activation energy of the rate-determining step of the four electron oxidation process, which results in a faster charge transfer to the electrolyte; this is the 'classical' role of an electrocatalyst. The second possible mechanism of a co-catalyst on a photoabsorber is the passivation of surface recombination centers and therefore the inhibition of surface recombination. Finally, as mentioned above, the co-catalyst can influence the band bending of the semiconductor by forming a Schottky-type junction, thereby enhancing the charge separation. As a result, we need a technique that can distinguish these different effects on the semiconductor/electrolyte and semiconductor/co-catalyst/electrolyte interfaces.

In this study, we use intensity modulated photocurrent spectroscopy (IMPS) to investigate the role of CoPi on spray-deposited BiVO$_4$ photoanodes.[5,13,14] With IMPS, the charge transfer and the surface recombination at the semiconductor/electrolyte interface can be clearly distinguished. This technique is increasingly utilized in the literature to understand the surface carrier dynamics at the semiconductor/electrolyte interface.[19–23] We will show that CoPi, despite being a dark electrocatalyst, does not enhance the charge transfer rate constant on the surface of BiVO$_4$, but instead suppresses surface recombination. Moreover, we find that a conventional electrocatalyst, such as RuO$_x$, does not significantly improve the photoactivity of BiVO$_4$, suggesting that BiVO$_4$ by itself is already thermodynamically active towards water oxidation. This conclusively shows that the photocurrent of BiVO$_4$ is limited by surface recombination, and not by slow oxygen evolution kinetics. The implications of these findings will be discussed.

Experimental

Preparation of BiVO$_4$ thin film photoanodes

Thin films of BiVO$_4$ were deposited by spray pyrolysis. Bi(NO$_3$)$_3$·5H$_2$O (98%, Alfa Aesar) and VO(AcAc) (99%, Alfa Aesar) were dissolved in acetic acid (98%, Sigma Aldrich) and absolute ethanol (Sigma Aldrich), respectively. The Bi solution was then added to the V solution (Bi : V = 1 : 1), and the mixture was diluted to 4 mM with excess ethanol. The acetic acid to ethanol volume ratio in the final solution is 1 : 9. The final solution was then ultrasonicated for 15 minutes. The FTO substrate was heated to 450 °C during deposition. The precursor solution was sprayed in a pulsed deposition mode onto the FTO, with one spray cycle consisting of 5 s spray time followed by 55 s delay time to allow the solvent to evaporate. After deposition, the films were annealed for 2 hours at 450 °C in air. More details can be found in previous reports.[24,25]

Co-catalyst deposition

The CoPi catalyst was electrodeposited (in the dark) on the surface of BiVO$_4$ in an electrochemical cell using a three-electrode configuration, according to the recipe from Kanan and Nocera.[7] The electrolyte is made by dissolving 0.5 mM Co(NO$_3$)$_2$·6H$_2$O (99%, Acros Organics) in a 0.1 M potassium phosphate (KPi) buffer solution (made by dissolving 0.034 M KH$_2$PO$_4$ and 0.066 M K$_2$HPO$_4$ to obtain pH ∼ 7). The potential of the working electrode was controlled by a potentiostat (EG&G PAR 283). A coiled Pt wire and an Ag/AgCl electrode (XR300, saturated KCl/AgCl solution, Radiometer Analytical) were used as the counter and reference electrodes, respectively. The electrodeposition was performed at a constant voltage of 1.1 V$_{NHE}$ (1.5 V$_{RHE}$) for 30 s. This resulted in a thickness of the Co–Pi layer of ∼1 nm.[24]

The RuO$_x$ catalyst was photoelectrodeposited on the surface of BiVO$_4$ in the same electrochemical cell that was used for the CoPi deposition. Based on the recipes from Gui and Tsuji,[26,27] an aqueous solution of 5 mM RuCl$_3$ (Ru content 45–55%, Sigma Aldrich) was used as the deposition bath with a pH ∼ 7. The photo-electrodeposition was performed under AM 1.5 illumination at a constant potential of 0.6 V$_{NHE}$ (1.0 V$_{RHE}$) for 400 s.

IMPS and photocurrent measurements

IMPS and photocurrent measurements were carried out in an aqueous solution of 0.1 M KPi (buffer, pH ∼ 7). The measurements were performed on bare and CoPi modified BiVO$_4$ films for a bias range of 0.6 to 1.5 V$_{RHE}$ and a frequency range of 0.1 Hz to 10 kHz. The electrochemical cell was the same as that used for the CoPi deposition, and was fitted with a quartz window to allow illumination of the sample surface. IMPS measurements were performed with modulated illumination provided by a light-emitting diode with a wavelength of 455 nm (Thorlabs M455L3) driven by an LED driver (Thorlabs DC2100). Using a beam splitter, the light was split into two beams: one onto the PEC cell, and the other onto a high-speed Si photodiode (Thorlabs PDA10A-EC). The signal output of a frequency response analyzer (FRA, Solartron 1250, Schlumberger) was used to modulate the light intensity sinusoidally, with an rms amplitude of 0.6 mW cm^{-2} superimposed on a 4 mW cm^{-2} DC background intensity. An EG&G PAR 283 potentiostat was used to control the potential, and its current monitor output was fed into the channel 1 of the FRA. The voltage signal of the high-speed Si photodiode was fed into the channel 2 of the FRA. The FRA then reported the real and imaginary components of the opto-electrical gain of the sample by dividing the measured photocurrent density (j_{photo}) through the voltage of the Si photodiode (channel 1/channel 2). This can be converted to the absolute (dimensionless) complex gain of the photoelectrode[28] by multiplying with a conversion factor. The conversion factor was determined by measuring the absolute intensity of the light using a calibrated photodiode (PD300UV + Ophir Nova II), and the voltage reading of the high-speed Si photodiode. The conversion factor for our setup was 0.00314 V cm^2 mA^{-1}. A schematic diagram of the setup is shown in Fig. 1.

The photocurrent–voltage measurements were performed using the same setup. The sample area is 0.283 cm^2. The 455 nm

LED light source (4 mW cm^{-2}) was chopped by applying a square wave with a frequency of 0.1 Hz. The number of absorbed photons in BiVO$_4$ at this wavelength and intensity is a factor of ~4 lower compared to full AM1.5 illumination, but this is still within the range of conditions encountered in practice when considering the effects of e.g. clouds.

The open circuit potential measurements as a function of light intensity were carried out using a combination of a 457 nm CW argon ion laser (Coherent Innova 90C Series) and multiple neutral density filters (metal film, OD 0.1–3, Melles Griot). The illumination intensities were measured with a calibrated photodiode (Ophir PD300-UV). Hydrogen peroxide (H$_2$O$_2$, 0.5 M) was added to the phosphate buffer to better define the redox potential of the electrolyte.

In situ UV-Vis measurements

The setup for the *in situ* UV-Vis measurements consists of a deuterium–halogen lamp (Mikropack DH-2000-BAL), which was used as the light source, an electrochemical cell with the sample under investigation (*e.g.*, BiVO$_4$, CoPi) as the working electrode, and a high sensitivity spectrometer (Ocean Optics Maya 2000 PRO) to measure the light transmitted through the sample. Optical fibers (Ocean Optics QP200-2-SR/BX) were used to guide the light from the deuterium–halogen lamp through the quartz window of the electrochemical cell and onto the spectrometer. The measured transmission spectra (integrated for 1 second) were divided by the reference spectrum (measured in the same cell prior to starting the experiment) to obtain the relative changes in the optical absorption (ΔA) as a function of applied potential and the wavelength of the light. The spectra were recorded while slowly scanning the potential, using a scan rate of 2 mV s^{-1}.

Theory

The water oxidation photocurrent in semiconductor photo-electrodes is a product of the illumination intensity, φ, the light harvesting efficiency, η_{LH}, the bulk charge separation efficiency, η_{CS}, and the charge-transfer efficiency from the semiconductor to the electrolyte, η_{CT} (sometimes called the injection efficiency).

$$J_{ph} = \varphi \eta_{LH} \eta_{CS} \eta_{CT} \qquad (1)$$

The η_{LH} is determined by the band gap and the absorption coefficient of the material. The η_{CS}, which is sometimes also called the hole collection efficiency, is defined as the fraction of the photogenerated holes that reaches the surface. Normally this is determined by the width of the space charge layer (SCL) and the minority carrier diffusion length, if we assume that no recombination occurs in the SCL. The η_{CT} in an n-type material is defined as the fraction of holes that transfers from the semiconductor into the electrolyte, and its value reflects the kinetic competition between charge transfer and surface recombination processes.

As mentioned earlier, the deposition of co-catalysts on the photoanode surface has been shown to either significantly improve the transfer efficiency (catalysis), to suppress the surface recombination, or to modify the band bending, all of which affects η_{CT} and/or η_{CS}. In order to determine which surface processes are affected, a measurement technique capable of de-convoluting the charge transfer processes is needed. When studying metal/electrolyte interfaces, methods based on potential variation, such as electrochemical imped-ance spectroscopy (EIS), are generally used to periodically modulate the reaction rates *via* the applied potential and in this way study the kinetics of charge transfer processes. However, these methods are not directly applicable for the semiconductor/electrolyte interface, since the potential varia-tions appear mainly across the space charge region of the semiconductor rather than across the Helmholtz layer. There-fore, in IMPS, a modulation of the light intensity is used to modulate the surface concentration of the photo-generated carriers. We thus modulate the concentration of one of the reactants instead of the reaction rate constant itself. A simpli-fied model, illustrated in literature by Peter *et al.*, is then used to analyze the competition between hole transfer (*i.e.*, hole injec-tion into the electrolyte) and surface recombination at the semiconductor/electrolyte interface. From this analysis, one can extract the values of the reaction rate constants for charge transfer, k_{tr}, and surface recombination, k_{rec}.[29] In the case of simple one-electron charge transfer reactions, these rate constants are true rate constants (s^{-1}). The situation is some-what more complicated for the case of multi-step charge transfer reactions. One can still use the same expressions to analyze the IMPS response and distinguish the hole injection and surface recombination processes, but k_{tr} and k_{rec} are now to be interpreted as phenomenological rate parameters that are functions of the rate constants of the elementary steps.[30,31] One can, in principle, derive these expressions if the reaction mechanism is known,[31] but so far this has not been attempted for the photo-oxidation of water by holes. We will therefore proceed with the understanding that k_{tr} and k_{rec} are to be interpreted as pseudo first-order rate constants.

The small amplitude modulation of the light intensity results in a modulation of the photocurrent with the same
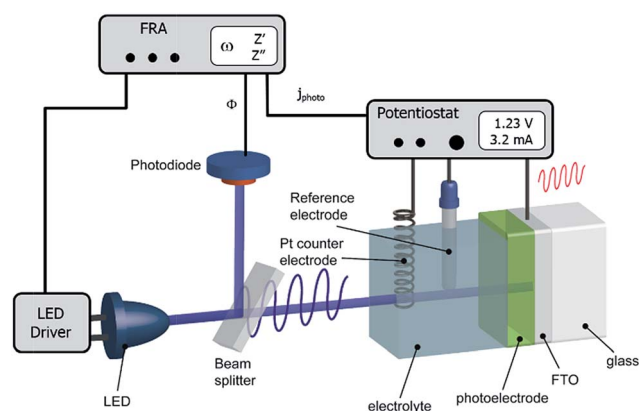

Fig. 1 Schematic diagram of the intensity modulated photocurrent spectroscopy (IMPS) setup. Modulated illumination is provided by a light emitting diode ($\lambda = 455$ nm), and the modulated photocurrent response of the sample is measured and analyzed.

frequency, but generally different magnitude and phase. The modulated photocurrent response consists of the sum of the hole current (minority carriers) and the electron current (majority carriers) that precedes the hole current. These in-phase and out-of-phase components result in a real and imaginary part of the photocurrent which can be plotted in a Nyquist plot. At low frequencies, this gives a semicircle that is located in the upper quadrant of the complex plane, see ESI Fig. S1.† This part is called the "recombination semicircle" because the shape of the semicircle is largely dominated by surface recombination. The imaginary photocurrent reaches a maximum when the frequency matches the characteristic relaxation constant of the system:

$$\omega_{\max} = k_{\text{tr}} + k_{\text{rec}} \quad (2)$$

As outlined above, k_{tr} and k_{rec} are the pseudo-first order charge transfer and recombination rate constants (s^{-1}), respectively. The high and low frequency intercepts of the x-axis (imaginary current = 0) are analogous to the initial maximum (spike) and the steady state photocurrents in a photocurrent transient plot, respectively.

At the high frequency intercept, the recombination is "frozen" due to fast modulation. Detailed analysis shows that the value at this intercept represents the product of the hole current, j_{h}, and the capacitance factor, $C_{\text{H}}/(C_{\text{SC}} + C_{\text{H}})$.[29] C_{SC} is the space charge capacitance, which can be estimated from the lower quadrant semicircle (ESI Fig. S1†) that represents the attenuation by the total series resistance of the cell and the combined space charge and Helmholtz capacitances of the sample, and is usually referred to as the RC time constant of the cell.[29] The frequency at the minimum of the semicircle, $\omega_{\min}$, corresponds to the product of the series resistance of the cell R_{cell} and C_{SC} ($\omega_{\min} = (R_{\text{cell}}C_{\text{SC}})^{-1}$). The Helmholtz capacitance C_{H} is assumed to be 20 $\mu\text{F cm}^{-2}$, but can usually even be neglected for standard materials with moderate charge carrier density.[32] This means that normalizing the photocurrent at this high frequency intercept against the hole current ($j_{\text{photo}}/j_{\text{h}}$) gives a value of $C_{\text{H}}/(C_{\text{SC}} + C_{\text{H}}) \approx 1$, when $C_{\text{SC}} \ll C_{\text{H}}$.

The low frequency intercept represents the fraction of the holes that arrive at the surface that is injected into the electrolyte. This is none other than the charge transfer efficiency,

$$\eta_{\text{CT}} = \frac{k_{\text{tr}}}{k_{\text{tr}} + k_{\text{rec}}} \quad (3)$$

It is important to note that the model is based on three main assumptions. First, bulk processes (e.g., band-to-band recombination, trapping) are assumed to be invisible. This is true if bulk recombination occurs before significant charge separation can take place, as the latter will lead to displacement currents. Since bulk recombination processes are much faster (typically <100 ns) than surface processes (typically 100 μs to 1 s), this assumption is likely to hold. Secondly, the relevant processes should occur on the same time scale as the IMPS measurements, which is indeed the case for most surface recombination processes.[1,4,33,34] Finally, the band bending is assumed to

remain constant during the modulated illumination. This is true if the space charge capacitance and the density of majority carriers do not change significantly during the modulation of the light intensity. For the modest modulation depth used in this study (15%), this assumption is also reasonable. Further details on the theory of IMPS can be found in the literature.[28,29,35,36]

Results and discussion

Fig. 2 shows the complex IMPS plot for bare BiVO₄ at different applied bias potentials. Each spectrum is normalized to ensure that the high frequency intercept with the real axis corresponds to $C_{\text{H}}/(C_{\text{SC}} + C_{\text{H}})$. As the applied bias is increased, the low frequency intercept also increases. Since the low frequency intercept represents the charge transfer efficiency ($k_{\text{tr}}/(k_{\text{tr}} + k_{\text{rec}})$), and recombination is expected to decrease at more positive potentials, this is as expected. The decrease in recombination at more positive potentials is also consistent with the overall increase of the photocurrent and the decrease of the transients in the chopped current–voltage curve shown in Fig. 3 (black curve).

Fig. 2 reveals that the high frequency semicircle of the photo response in the lower quadrant (the RC attenuation semicircle) is somewhat flattened. The same observation on hematite has been attributed to the frequency-dependence of the dielectric constant and/or surface inhomogeneities.[20] A similar explanation may hold here, as our spray-deposited films show some roughness with typical feature sizes of ∼100 nm.[37]

Using eqn (2) and (3), the charge transfer rate constant, k_{tr}, and the surface recombination rate constant, k_{rec}, are calculated from the IMPS spectra of un-modified and CoPi-modified BiVO₄. Fig. 4 shows the results as a function of applied potential. We first analyze the bare BiVO₄ and observe two potential ranges with different behaviors. At potentials below 1 V_{RHE}, k_{rec} is constant whereas k_{tr} increases with increasing potential. The
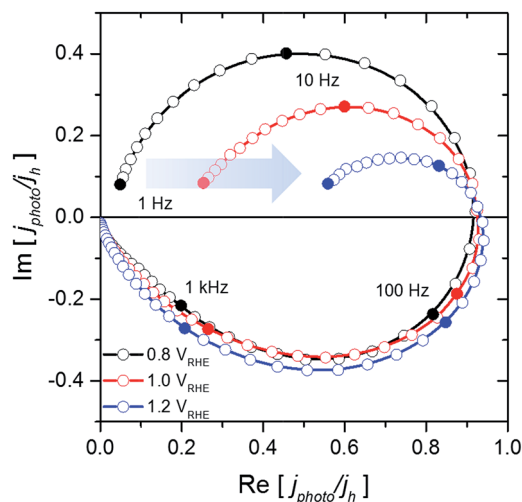

Fig. 2 IMPS spectra of BiVO₄ photoanode under different applied potentials. The increase of low-frequency intercepts with increasing potential, indicate an improvement of the charge transfer efficiency.
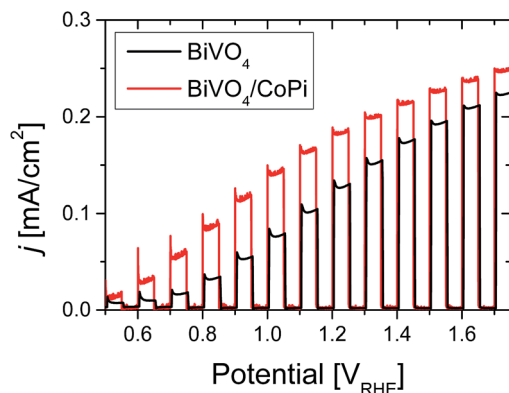
Fig. 3 Photocurrent–voltage (j–V) curve of bare BiVO$_4$ (black) and CoPi modified BiVO$_4$ (red) taken under chopped illumination with a 455 nm LED ($\Phi = 4$ mW cm^{-2}).

constant k_{rec} suggests that the band bending does not change in this potential regime. Any change in the applied bias thus has to fall across the Helmholtz layer. This is indeed consistent with the observed increase in k_{tr} with potential. Although this resembles metallic behavior (ESI Fig. S2a†), it is highly unlikely that these (undoped) BiVO$_4$ films are truly metallic in nature. Instead, we attribute the behavior of k_{rec} and k_{tr} to Fermi level pinning at the BiVO$_4$ surface (ESI Fig. S2b†).

For potentials more positive than 1 V$_{RHE}$, the photoanode is behaving more like a 'normal' semiconductor (ESI Fig. S2c†). Most of the change in the applied bias falls across the space charge region, which affects the concentration of conduction band electrons and, therefore, k_{rec}. In this regime, k_{tr} does not depend on the applied potential, which is indeed expected for a semiconductor/liquid junction. To further support these observations, the (external) quantum efficiency (EQE) is plotted as $-\ln(1 - \text{EQE})$ as a function of the square root of the applied potential with respect to the flatband potential (ESI Fig. S3†). At potentials > 1 V$_{RHE}$, $-\ln(1 - \text{EQE})$ is found to be proportional to the square root of the potential difference. This is in good agreement with the Gärtner equation,[38] which expresses the photocurrent for an ideal planar Schottky-type junction:

$$j_h = q I_0 \left(1 - \frac{e^{-\alpha W}}{1 + \alpha L_p} \right) \qquad (4)$$

$$-\ln(1 - \text{EQE}) = \alpha W + \ln(1 + \alpha L_p) \qquad (5)$$

with

$$W = \sqrt{\frac{2\varepsilon_0 \varepsilon_r}{q N_D} \left(\phi_{sc} - \frac{kT}{q} \right)} \qquad (6)$$

here, j_h is the hole current that arrives at the surface, I_0 is the incident photon flux, α is the absorption coefficient of the film, W is the width of the space charge region, and L_p is the hole diffusion length. ε_0 and ε_r are the vacuum permittivity and dielectric constant, respectively, q is the elementary charge, N_D is the donor density, φ_{sc} is the potential drop across the space charge layer ($\varphi_{sc} = V_{applied} - V_{FB}$), k is the Boltzmann constant,
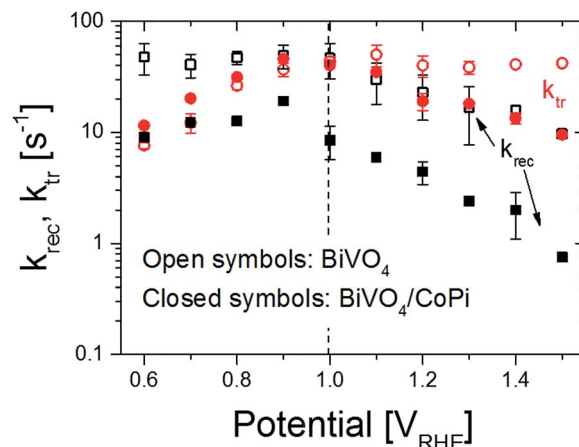

Fig. 4 Charge transfer rate constant (red) and recombination rate constant (black) for the unmodified (open symbols) and the CoPi modified BiVO$_4$ (closed symbols). The error bars represent the spread in the results obtained for different samples at selected potentials; in total, three bare BiVO$_4$ electrodes and two BiVO$_4$/CoPi electrodes were measured.

and T is the temperature. This ideal behavior implies that the Fermi level is no longer pinned at potentials positive of 1 V$_{RHE}$.

After modification with CoPi, k_{rec} and k_{tr} show very different behavior (Fig. 4, closed symbols). Most notably, the surface recombination rate constant is suppressed by a factor of 10–20 over the entire potential range. One possible explanation would be a change in band bending due to the formation of a Schottky-like contact between BiVO$_4$ and CoPi. This in turn would affect the concentration of electrons at the surface (n_s), and thus also the surface recombination rate constant. If this were the case, one would expect to observe a higher value of the high frequency photocurrent intercept with the real axis of the IMPS spectra, which corresponds to the flux of holes arriving at the surface before they have a chance to recombine (at these frequencies, recombination is 'frozen'). A change in band bending would affect the width of the depletion region (where charge separation occurs), and thus the amount of photo-generated holes that reach the surface. As shown in Fig. S4,† no significant difference in the high-frequency photocurrent intercept with the real axis is observed for bare and CoPi modified BiVO$_4$. To further study the possibility of a change in band bending upon adding CoPi in more detail, we measured the change of the open circuit potential upon illumination (ΔOCP) using a high intensity cw Ar ion laser source (ESI Fig. S5†). The ΔOCP is found to increase by only a small amount (~24 mV) after adding the CoPi, independent of the light intensity. A 24 mV change in the surface band bending corresponds to a ~2.5-fold decrease of surface majority carrier concentration, which is much lower than the observed ~15-fold decrease of the surface recombination rate constant. Thus, while a small change in band bending is indeed observed, we conclude that it plays only a very minor (if any) role in suppressing the recombination in CoPi modified BiVO$_4$.

An alternative explanation for the decrease in k_{rec} is that CoPi passivates the surface defects at which recombination occurs.

Although the chemical nature of these surface defects and the mechanism by which passivation of such states by CoPi would occur is not clear at this stage, our observations are consistent with such a passivation mechanism.

For a more detailed analysis of the influence of CoPi, we first look at the behavior of CoPi-modified BiVO$_4$ at modest applied potentials (<1 V$_{RHE}$). The overall trends in Fig. 4 are the same as for bare BiVO$_4$, i.e., k_{tr} increases with potential and k_{rec} remains constant. This suggests that Fermi level pinning still occurs at the BiVO$_4$/CoPi surface and that the surface states that are responsible for the Fermi level pinning are not passivated by the CoPi. Within this potential range, k_{rec} is reduced by the introduction of CoPi; this is attributed to surface passivation, as discussed above. However, the presence of CoPi does not affect the value of k_{tr}. This is not what one would intuitively expect, since CoPi is expected to act as an electrocatalyst and should thus enhance the charge transfer rate. Instead, the negligible change in k_{tr} suggests that the charge transfer still occurs via the BiVO$_4$ surface. This is consistent with the recent findings of Ma et al.; based on their transient photocurrent/absorption studies, these authors also suggest that charge transfer still predominantly occurs via the BiVO$_4$ in a CoPi-catalyzed BiVO$_4$ film.[39] This is actually not so surprising since the oxidation power (i.e., thermodynamic driving force) of holes in the valence band of BiVO$_4$ is higher than that of holes in CoPi. Specifically, the overpotential of CoPi is reported to be ~0.3–0.4 V, whereas the valence band of BiVO$_4$ is located more than 1 V positive of the water oxidation potential.[7,40–42]

At potentials >1.0 V$_{RHE}$, the recombination rate constant of the CoPi-modified BiVO$_4$ is again greatly reduced. However, the charge transfer rate constant, k_{tr}, decreases with increasing potential. We tentatively attribute this counter-intuitive observation to a gradual shift of direct water oxidation at the BiVO$_4$ surface (high driving force) to oxidation via CoPi at more positive potentials. The reason for this shift is that the exposed BiVO$_4$ surface, which is not very catalytically active, can no longer keep up with the increasing flux of photogenerated holes. As a result, an increasing fraction of these holes will now oxidize the CoPi. Although the latter has been reported to have a much higher intrinsic catalytic activity[7,43] than the BiVO$_4$ surface, the thermodynamic overpotential available for water oxidation for holes in CoPi is much lower than it is for holes in the BiVO$_4$ valence band. This would explain the decrease in k_{tr} with increasing potential.

To support this tentative model, we monitored the oxidation of CoPi as a function of the applied potential by in situ UV-Vis absorption measurements. The oxidation of CoPi leads to an absorption around 350 nm (Fig. S6a†), while control experiments confirm that no optical changes occur for bare FTO (Fig. S6c†) or for FTO/BiVO$_4$ (Fig. S6d†). The absorption data for FTO/BiVO$_4$/CoPi, shown in Fig. S6b,† reveal that CoPi starts to oxidize at potentials above ~0.8 V$_{RHE}$. This is close to the potential at which k_{tr} for CoPi-modified BiVO$_4$ starts to decrease (Fig. 4), and is consistent with our hypothesis (and the recent work of Ma et al.[39]) that water oxidation indeed shifts gradually from the BiVO$_4$ surface to the CoPi.

The IMPS data clearly indicate that surface recombination limits the photocurrent of bare BiVO$_4$, and that a CoPi layer enhances the photocurrent by passivating surface recombination centers. Although CoPi is well-known to be an efficient (dark) electrocatalyst, this does not seem to be its main function in the BiVO$_4$/CoPi system. To further support the assertion that the photocurrent of BiVO$_4$ is limited by surface recombination, we modified BiVO$_4$ photoelectrodes with RuO$_x$ particles. RuO$_x$ is known to be an excellent water oxidation catalyst. If BiVO$_4$ is not limited by hole transfer properties, modifying the surface with RuO$_x$ should not increase the charge transfer rate constant, k_{tr}. In fact, k_{tr} is expected to decrease due to the lower oxidation power of holes in RuO$_x$ compared to holes in the valence band of BiVO$_4$. To test this prediction, we deposited RuO$_x$ onto BiVO$_4$ photoanodes. We used a photo-assisted anodic process to ensure that the RuO$_x$ is deposited on the surface facets where the photo-generated holes arrive and do their electrochemical work. We also deposited RuO$_x$ on FTO to verify its high catalytic activity, see ESI Fig. S7.† Fig. 5a shows that the photocurrent of BiVO$_4$ does indeed not improve with the introduction of RuO$_x$; it actually decreases. Moreover, Fig. 5b shows that the charge transfer rate constant is actually smaller than that of the bare BiVO$_4$. The surface recombination is not affected, which shows that RuO$_x$ does not passivate the BiVO$_4$ surface. These
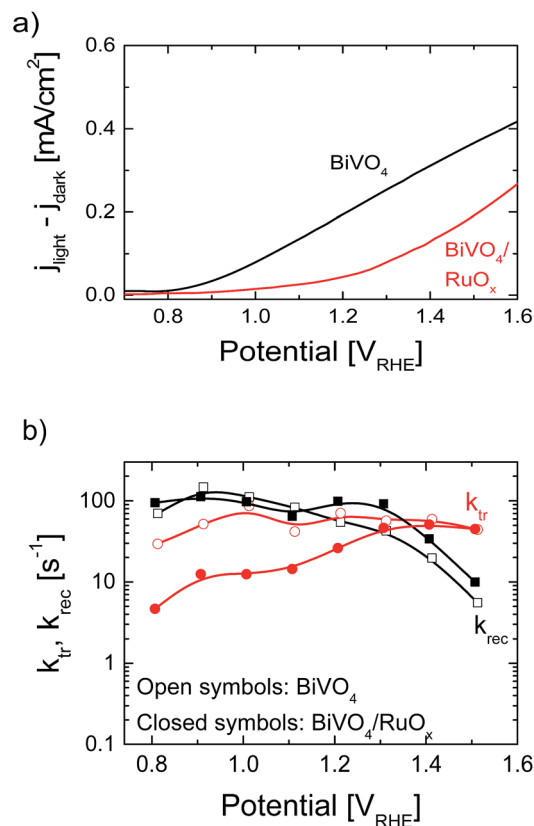

Fig. 5 (a) Photocurrent−voltage (j−V) curve of bare BiVO$_4$ (black) and RuO$_x$ modified BiVO$_4$ (red) taken under illumination with a 455 nm LED ($\varphi = 4$ mW cm^{-2}). (b) Charge transfer rate (red) and recombination rate constant (black) for the unmodified (open symbols) and the RuO$_x$ modified BiVO$_4$ (closed symbols).

observations are fully consistent with our model and confirm our hypothesis that the photocurrent of $BiVO_4$ is limited by surface recombination, not water oxidation kinetics.

It should be pointed out that $BiVO_4$ samples prepared by different methods may be limited by other factors. For example, undoped $BiVO_4$ samples made by RF magnetron sputtering consistently show lower onset potentials and higher injection efficiencies than sprayed samples.[44] Efforts to improve these sputtered samples by CoPi or RuO_x deposition have been unsuccessful (unpublished results), most likely because their performance is limited by bulk recombination at sputter-induced defects.[44] For the spray-deposited samples studied here, however, surface recombination is clearly the main performance-limiting factor.

Our understanding of the processes taking place at the bare and co-catalyst modified $BiVO_4$ is summarized in Fig. 6. For the bare $BiVO_4$ shown in Fig. 6a, the valence band holes can either directly oxidize water (1), or move to the surface states and recombine with conduction band electrons (2). The latter means that they do not participate in water oxidation. By functionalizing the $BiVO_4$ with a surface passivating "co-catalyst", such as CoPi, the surface state is passivated (Fig. 6b). This effectively blocks the surface recombination pathway for the valence band holes, which will instead be injected into the electrolyte to directly oxidize water. We note that the CoPi layer

is porous, so part of the $BiVO_4$ is still in direct contact with water. With increasing potentials, however, the surface of $BiVO_4$ can no longer keep up with the photogenerated hole flux, due to its low intrinsic catalytic activity (slow kinetics). This limits the direct injection of holes into the electrolyte (1), and favors the competing pathway of hole transfer to the CoPi (3). Here, the intrinsic (catalytic) activity for water oxidation is higher, but the thermodynamic driving force is much smaller, which leads to an overall decrease in k_{tr} with applied potential, as described above in detail. Finally, a non-passivating co-catalyst, such as RuO_x, on $BiVO_4$ (Fig. 6c) does not affect the recombination rate constant. The RuO_x does, however, decrease the k_{tr} compared to $BiVO_4$ due to the lower oxidation power of the holes in RuO_x.

Conclusions

Using IMPS, we have shown that modification of the surface of sprayed $BiVO_4$ photoanodes with CoPi reduces surface recombination with a factor of 10–20. The charge transfer rate constant is much less affected, which is surprising in view of the fact that CoPi is a well-known electrocatalyst. The resulting increase in the overall charge transfer efficiency is consistent with the observed increase in photocurrent. Moreover, surface modification with RuO_x, one of the best known OER catalysts, does not lead to an increase in the photocurrent. These results provide compelling evidence that the main role of CoPi on $BiVO_4$ is not to enhance the water oxidation kinetics, but to suppress surface recombination. We emphasize that this conclusion is not absolute and recognize that there may be conditions under which CoPi indeed functions as an OER catalyst (as we suggested during the discussion of Fig. 6b).

Our conclusion also implies that the photocurrent of $BiVO_4$ is not limited by surface reaction kinetics, but by surface recombination. Similar conclusions have recently been drawn for CoPi-catalyzed hematite electrodes[8] which, perhaps in hindsight, is not so surprising when one considers the strong oxidizing power of the valence band holes in most wide-bandgap metal oxide semiconductors. The importance of surface recombination is very well recognized and established in the field of photovoltaics, but much less so in photo-electrochemistry and photocatalysis. At the moment it is unclear whether surface recombination is particular to $BiVO_4$ (and perhaps certain types of α-Fe_2O_3), or if it is a more generally occuring limitation in oxide semiconductors. The same is true for the passivating behavior of CoPi; this "catalyst" may also be able to passivate other photoanode materials, and it is likely that there are also other materials that are able to passivate $BiVO_4$ and Fe_2O_3. Further development of efficient photoelectrochemical solar fuel generators clearly requires a better understanding of semiconductor/catalyst systems and the processes that occur at these interfaces.
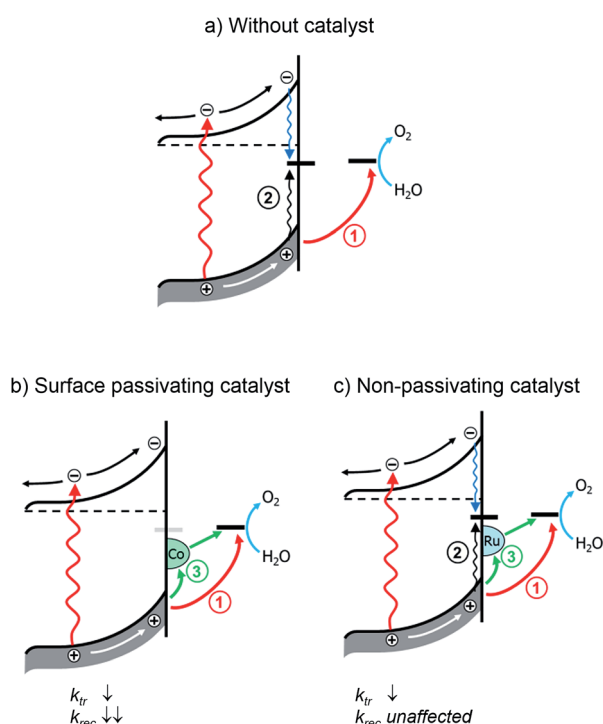

Fig. 6 Simplified model of the elementary processes in a $BiVO_4$ photoanode (a) without a co-catalyst (b) with a surface passivating co-catalyst (*e.g.* CoPi) and (c) with a non-passivating co-catalyst (*e.g.* RuO_x). Upon illumination, photo-excited carriers move towards the semiconductor–electrolyte interface, where direct water oxidation by valence band holes (1), surface state-mediated recombination (2), and charge transfer *via* co-catalyst (3) can take place.

Acknowledgements

Notes and references

1 Y. Ma, S. R. Pendlebury, A. Reynal, F. Le Formal and J. R. Durrant, *Chem. Sci.*, 2014, **5**, 2964.

2 Y. Park, K. J. McDonald and K.-S. Choi, *Chem. Soc. Rev.*, 2013, **42**, 2321–2337.

3 T. W. Kim and K.-S. Choi, *Science*, 2014, **343**, 990–994.

4 Y. Ma, F. Le Formal, A. Kafizas, S. R. Pendlebury and J. R. Durrant, *J. Mater. Chem. A*, 2015, **3**, 20649–20657.

5 D. K. Zhong, S. Choi and D. R. Gamelin, *J. Am. Chem. Soc.*, 2011, **133**, 18370–18377.

6 L. Trotochaud, S. L. Young, J. K. Ranney and S. W. Boettcher, *J. Am. Chem. Soc.*, 2014, **136**, 6744–6753.

7 M. W. Kanan and D. G. Nocera, *Science*, 2008, **321**, 1072–1075.

8 D. R. Gamelin, *Nat. Chem.*, 2012, **4**, 965–967.

9 M. Barroso, C. A. Mesa, S. R. Pendlebury, A. J. Cowan, T. Hisatomi, K. Sivula, M. Grätzel, D. R. Klug and J. R. Durrant, *Proc. Natl. Acad. Sci. U. S. A.*, 2012, **109**, 15640–15645.

10 Y.-R. Hong, Z. Liu, S. F. B. S. A. Al-Bukhari, C. J. J. Lee, D. L. Yung, D. Chi and T. S. A. Hor, *Chem. Commun.*, 2011, **47**, 10653.

11 C. Y. Cummings, F. Marken, L. M. Peter, A. A. Tahir and K. G. U. Wijayantha, *Chem. Commun.*, 2012, **48**, 2027.

12 J. A. Seabold and K. S. Choi, *Chem. Mater.*, 2011, **23**, 1105–1112.

13 F. F. Abdi, L. Han, A. H. M. Smets, M. Zeman, B. Dam and R. van de Krol, *Nat. Commun.*, 2013, **4**, 1–7.

14 H. Ye, H. S. Park and A. J. Bard, *J. Phys. Chem. C*, 2011, **115**, 12464–12470.

15 M. Higashi, K. Domen and R. Abe, *J. Am. Chem. Soc.*, 2012, **134**, 6968–6971.

16 Y. Liu, Y. Zhou, G. Chen, T. Guo, L. Wang, X. Huang and W. Zeng, *Mater. Lett.*, 2015, **148**, 155–158.

17 B. Klahr, S. Gimenez, F. Fabregat-Santiago, J. Bisquert and T. W. Hamann, *Energy Environ. Sci.*, 2012, **5**, 7626.

18 F. Lin and S. W. Boettcher, *Nat. Mater.*, 2014, **13**, 81–86.

19 H. K. Dunn, J. M. Feckl, A. Müller, D. Fattakhova-Rohlfing, S. G. Morehead, J. Roos, L. M. Peter, C. Scheu and T. Bein, *Phys. Chem. Chem. Phys.*, 2014, **16**, 24610–24620.

20 L. M. Peter, K. G. U. Wijayantha and A. A. Tahir, *Faraday Discuss.*, 2012, **155**, 309–322.

21 W. Li, D. He, S. W. Sheehan, Y. He, J. E. Thorne, X. Yao, G. W. Brudvig and D. Wang, *Energy Environ. Sci.*, 2016, **9**, 1794–1802.

22 J. E. Thorne, J.-W. Jang, E. Y. Liu and D. Wang, *Chem. Sci.*, 2016, **7**, 3347–3354.

23 G. Liu, S. Ye, P. Yan, F. Xiong, P. Fu, Z. Wang, Z. Chen, J. Shi and C. Li, *Energy Environ. Sci.*, 2016, **9**, 1327–1334.

24 F. F. Abdi and R. van de Krol, *J. Phys. Chem. C*, 2012, **116**, 9398–9404.

25 F. F. Abdi, N. Firet, A. Dabirian and R. van de Krol, *MRS Proc.*, 2012, **1446**, DOI: 10.1557/opl.2012.811.

26 Z. Gui, E. Gillette, J. Duay, J. Hu, N. Kim and S. B. Lee, *Phys. Chem. Chem. Phys.*, 2015, **17**, 15173–15180.

27 E. Tsuji, A. Imanishi, K. I. Fukui and Y. Nakato, *Electrochim. Acta*, 2011, **56**, 2009–2016.

28 L. Peter and L. Peter, *Chem. Rev.*, 1990, **90**, 753–769.

29 E. A. Ponomarev and L. M. Peter, *J. Electroanal. Chem.*, 1995, **396**, 219–226.

30 D. J. Fermín, E. A. Ponomarev and L. M. Peter, *J. Electroanal. Chem.*, 1999, **473**, 192–203.

31 L. M. Peter, E. A. Ponomarev and D. J. Fermin, *J. Electroanal. Chem.*, 1997, **427**, 79–96.

32 R. van de Krol and M. Grätzel, *Photoelectrochemical Hydrogen Production*, Springer-Verlag, 2012.

33 F. Le Formal, K. Sivula and M. Grätzel, *J. Phys. Chem. C*, 2012, **116**, 26707–26720.

34 S. R. Pendlebury, A. J. Cowan, M. Barroso, K. Sivula, J. Ye, M. Grätzel, D. R. Klug, J. Tang and J. R. Durrant, *Energy Environ. Sci.*, 2012, **5**, 6304–6312.

35 J. Li and L. M. Peter, *J. Electroanal. Chem.*, 1985, **193**, 27–47.

36 R. Peat and L. M. Peter, *J. Electroanal. Chem.*, 1987, **228**, 351–364.

37 F. F. Abdi, N. Firet and R. van de Krol, *ChemCatChem*, 2013, **5**, 490–496.

38 W. W. Gärtner, *Phys. Rev.*, 1959, **116**, 3.

39 Y. Ma, A. Kafizas, S. R. Pendlebury, F. Le Formal and J. R. Durrant, *Adv. Funct. Mater.*, 2016, **26**, 4951–4960.

40 K. Ding, B. Chen, Y. Li, Y. Zhang and Z. Chen, *J. Mater. Chem. A*, 2014, **2**, 8294.

41 S. Kohtani, K. Yoshida, T. Maekawa, A. Iwase, A. Kudo, H. Miyabe and R. Nakagaki, *Phys. Chem. Chem. Phys.*, 2008, **10**, 2986.

42 R. Saito, Y. Miseki and K. Sayama, *Chem. Commun.*, 2012, **48**, 3833.

43 C. C. L. McCrory, S. Jung, J. C. Peters and T. F. Jaramillo, *J. Am. Chem. Soc.*, 2013, **135**, 16977–16987.

44 H. Gong, N. Freudenberg, M. Nie, R. van de Krol and K. Ellmer, *AIP Adv.*, 2016, **6**, 45108.